ELSEVIER

Tectonophysics 274 (1997) 117–143

TECTONOPHYSICS

Shear concentration in a collision zone: kinematics of the Chihshang Fault as revealed by outcrop-scale quantification of active faulting, Longitudinal Valley, eastern Taiwan

J. Angelier [a,*], H.-T. Chu [b], J.-C. Lee [c]

[a] *Tectonique Quantitative, Dép. de Géotectonique and U.R.A. 1759, University P. and M. Curie, Bôte 129, 4 pl. Jussieu, 75252 Paris Cedex 05, France*

[b] *Central Geological Survey, M.O.E.A., Taipei, Taiwan*

[c] *Institute of Earth Sciences, Academia Sinica, P.O. Box 1-55, Nankang, Taipei, Taiwan*

Received 15 April 1996; accepted 24 July 1996

Abstract

Repeated measurements of active deformation were carried out at three sites along the active Chihshang Fault, a segment of the Longitudinal Valley Fault zone of eastern Taiwan (the present-day plate boundary between the Philippine Sea Plate and Eurasia). Reliable annual records of displacement along an active fault, were obtained based on detailed surveys of faulted concrete structures. Along the active Chihshang Fault striking N18ºE, we determined average motion vectors trending N37ºW with an average shortening of 2.2 cm/yr. Thus, the transverse component of motion related to westward thrusting is 1.8 cm/yr, whereas the left-lateral strike-slip component of motion is 1.3 cm/yr. The fault dips 39–45º to the east, so that the vertical displacement is 1.5–3 cm/yr and the actual oblique offset of the fault increases at a rate of 2.7–3.7 cm/yr. This is in good agreement with the results of regional geodetic and tectonic analyses in Taiwan, and consistent with the N54ºW trend of convergence between the northernmost Luzon Arc and South China revealed by GPS studies. Our study provides an example of extreme shear concentration in an oblique collision zone. At Chihshang, the whole horizontal shortening of the Longitudinal Valley Fault, 2.2 cm/yr on average, occurs across a single, narrow fault zone, so that the whole reverse slip (about 2.7–3.7 cm/yr depending on fault dip) was entirely recorded by walls 20–200 m long where faults are tightly localized. This active faulting accounts for more than one fourth (27%) of the total shortening between the Luzon Arc and South China recorded through GPS analyses. Further surveys should indicate whether the decreasing shortening velocity across the fault is significant (revealing increasing earthquake risk due to stress accumulation) or not (revealing continuing fault creep and 'weak' behaviour of the Chihshang Fault).

Keywords: active fault; seismotectonics; geodesy; earthquake risk; kinematics; shear; collision; Taiwan

1. Introduction

In eastern Taiwan, the Longitudinal Valley Fault zone is the main active boundary between Eurasia and the Philippine Sea Plate (Fig. 1). The Longitudinal Valley Fault is the surface expression of a major shear zone striking N20ºE and dipping approximately 55º to the ESE; it is followed along strike over a distance of about 160 km, and along dip at depths of at least 45 km. This major fault

* Corresponding author.

PII S0040-1951(96)00301-0

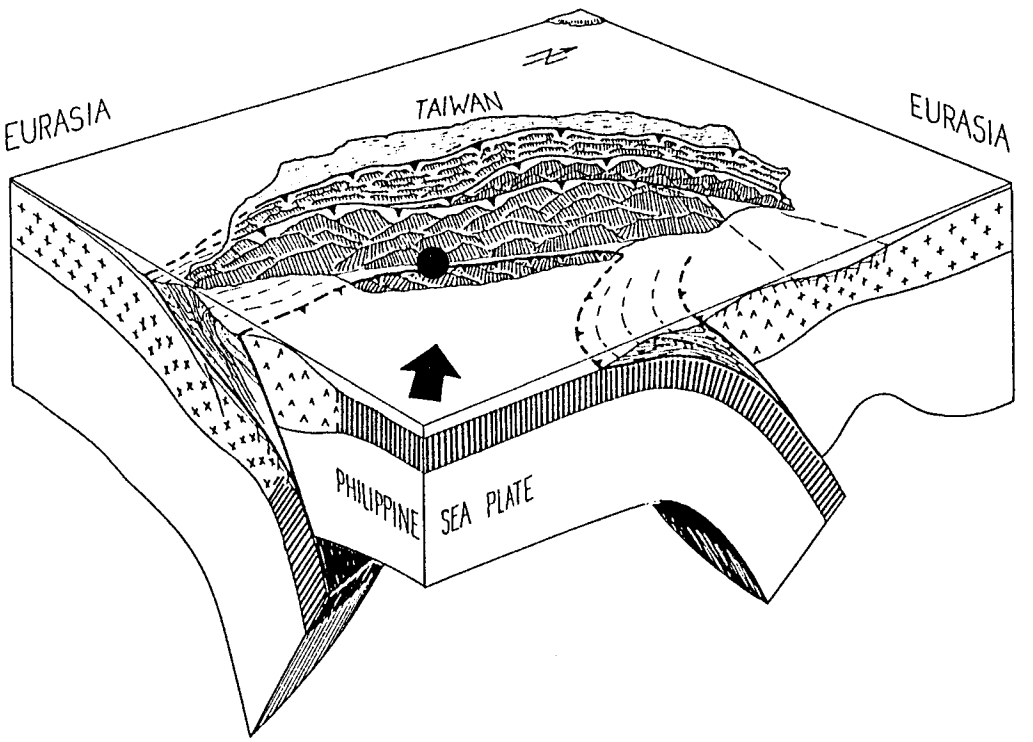

Fig. 1. The Longitudinal Valley Fault of Eastern Taiwan as the present-day plate boundary between the Philippine Sea Plate and Eurasia. Location within the lithospheric pattern of the Taiwan collision zone (after Angelier, 1986, modified), between the subduction zones of the Ryukyu arc-and-trench (on right) and the Manila Trench–Luzon Arc (on left). Oceanic crust, hachured pattern. Continental crust, pattern of crosses. Island-arc crust, pattern of overturned 'v's. Lithospheric mantle left white. Large black arrow: northwestward movement of the Philippine Sea Plate relative to Eurasia. Large black dot: location of the Chihshang Fault, along the Longitudinal Valley Fault.

zone separates the Central Range (the deformed Chinese margin to the west) and the Coastal Range (the northernmost segment of the Luzon Arc).

Earlier studies highlighted the geodynamic significance of this major boundary (Ho, 1986; Tsai, 1986). We focus on a quantitative analysis of present-day activity. We carried out determinations of displacement during the period 1982–1994 along an active segment of the Longitudinal Valley Fault: the Chihshang Fault (Fig. 2). Near Chihshang, in addition to morphological, seismological and geodetic evidences for active faulting, present-day offsets can be measured in the field using relatively simple techniques, so that the evolution of motion on a single fault surface could be accurately studied at the time scale of a few years.

The purpose of this paper is twin-fold. From the methodological point of view, we aim at demonstrating that it is possible to accurately quantify active fault kinematics despite difficulties related to tropical climate. From the geodynamic point of view, we aim at comparing these kinematic determinations on a single major fault with the geodetic estimates of deformation independently obtained for the whole Longitudinal Valley fault zone, several km wide, and also for the whole collision zone of Taiwan, approximately 100 km wide.

2. The active Chihshang Fault

The Longitudinal Valley of eastern Taiwan (Fig. 2) was recognized a long time ago as a major site of active faulting (Hsu, 1962) and seismic activity (Yu and Tsai, 1982). Based on geodetic surveys, estimates of shortening averaged 2 cm/yr (Yu and Liu, 1989; Yu et al., 1990). Earthquakes and active faulting were described by Hsu (1962), York (1976) and Bonilla (1977). Active faulting principally occurs on

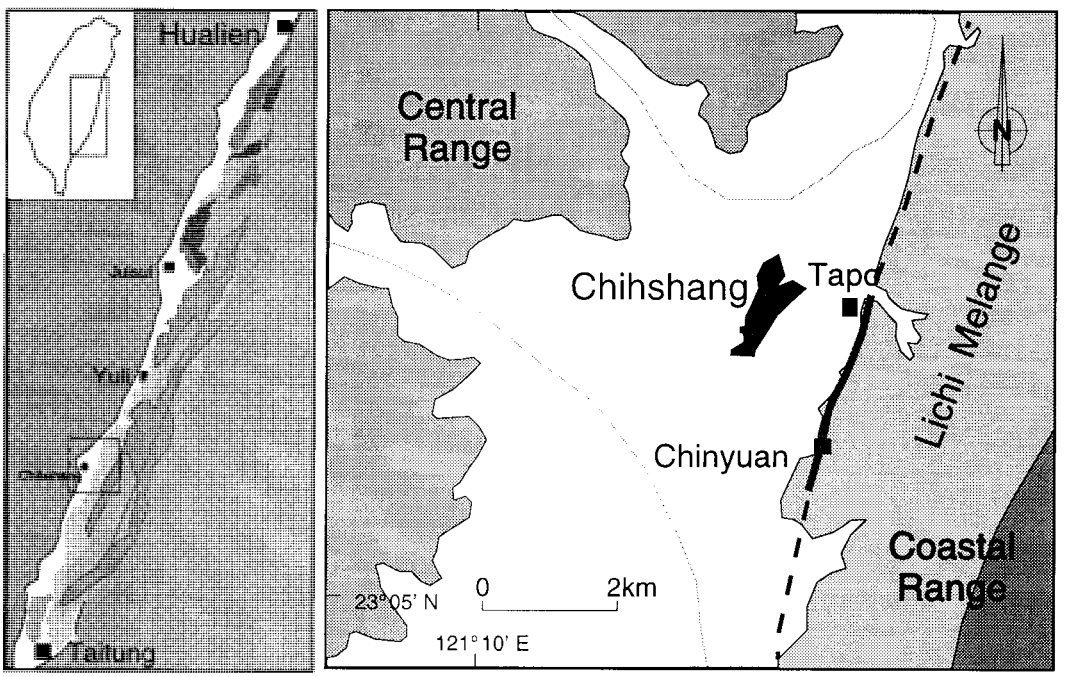

Fig. 2. Simplified geological map of the Chihshang Fault area. On left, location in Taiwan (small frame: location of the map on right); Longitudinal Valley left white between the Central Range of Taiwan (to the west) and the Coastal Range (to the east). On right, map of Chihshang area. Main geological formations, from west to east: metamorphic basement of the Central Range, late Quaternary alluvions of the Longitudinal Valley (left white), Pliocene Lichi Mélange (commonly overlain by Quaternary terraces) and late Neogene formations of the Coastal Range. Active fault trace: thick line.

the eastern side of the Longitudinal Valley, near the contact with the Coastal Range. Large earthquakes occurred at various places along the Longitudinal Valley, such as in 1951 (Meilun near Hualien, magnitude $M_S = 7.1$; Yuli, $M_S = 5.3$), 1972 (Juisui, $M_S = 6.9$) and 1986 (Hualien, $M_S = 6.4$ and 7.8). Considering the high average rate of motion across this major fault zone, the frequency and importance of earthquakes are much less than could be expected. Although fractures appeared in the ground and buildings along the Chihshang Fault in November 1951, during the Taitung earthquakes, it was observed that numerous fractures also developed in the absence of large earthquakes.

Records of elevation changes as well as seismological analyses indicate that the Yuli segment of the Longitudinal Valley Fault is the most active (M.-S. Yu et al., 1995). The Chihshang Fault (Fig. 2), a southern portion of the Yuli segment, has a length of few tens of kilometres and strikes N18ºE. Around Chihshang, analyses of trilateration networks during the period 1983–1988 revealed NW–SE shortening of about 2 cm/yr. Geodetic levelling along E–W profiles during the period 1986–1988 showed that the western side of the Coastal Range was uplifted at a rate of about 2 cm/yr, while the Longitudinal Valley was subsiding at a rate of about 1 cm/yr (Yu and Liu, 1989). The Chihshang Fault is known to have been active during the last 30 years, leaving numerous fractures in walls, roads and buildings along the western boundary of the Coastal Range. Earthquakes occur, but creeping prevails.

The active Chihshang Fault is located in front of one of the two major water divides of the Longitudinal Valley (the other divide being at a distance of about 80 km to the north). This topographic high is accentuated by the presence of a major alluvial fan at the foot of the Central Range (Fig. 3). It is also related to a zone of relative uplift which coincides with the longitudinal extent of the active Chihshang Fault. We infer that the present-day downward motion of the Longitudinal Valley, as revealed by levelling

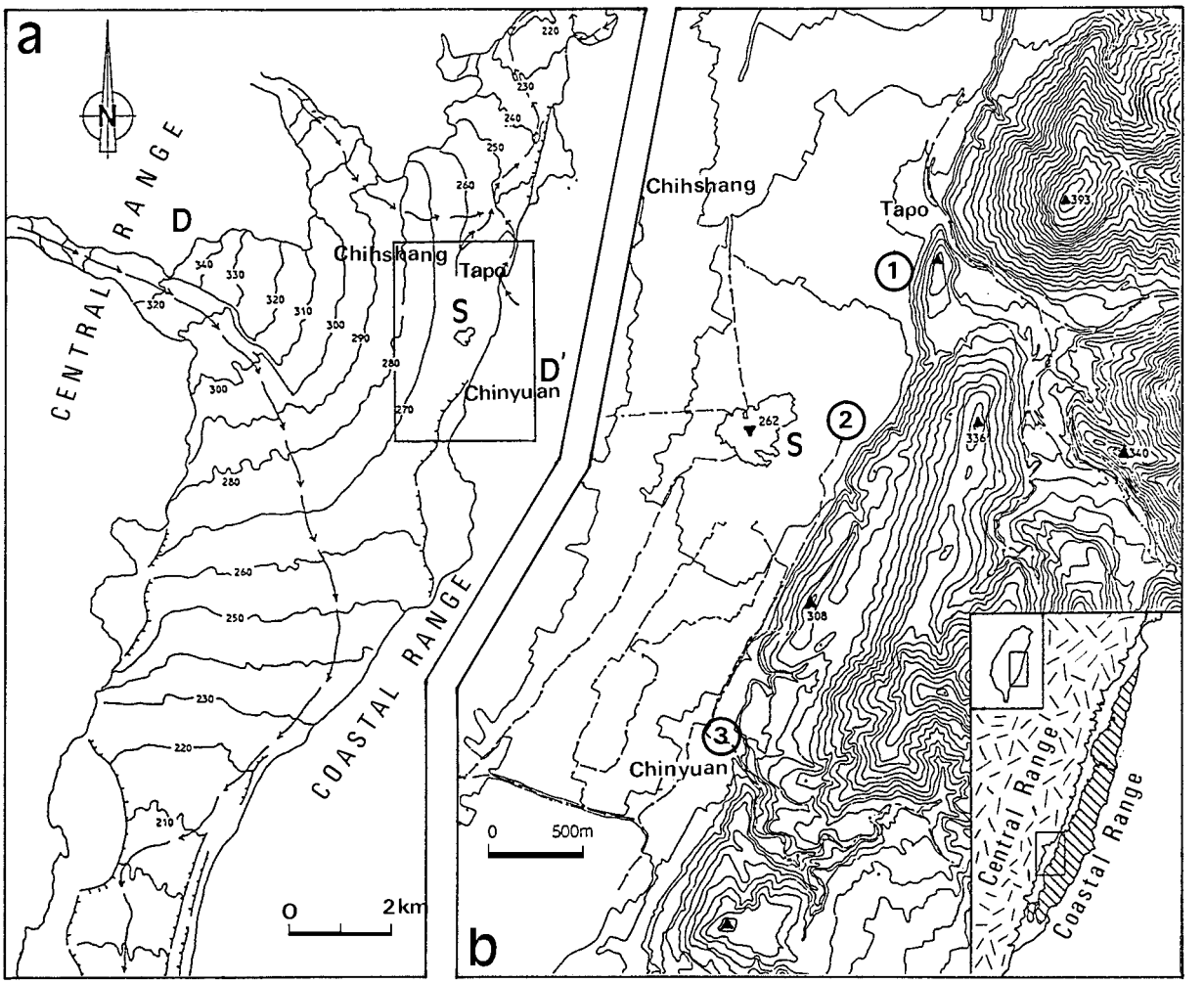

Fig. 3. Morphological characteristics of the Chihshang Fault area. (a) Topography and drainage pattern of the Longitudinal Valley in front of the Chihshang Fault. Elevations in metres (isocontour interval: 10 m), shown in late Quaternary alluvions solely. Main rivers shown as dashed lines with downstream-directed arrows. Scarps along Quaternary terraces shown as lines with barbs on the lower side. *D–D′*: location of the Chihshang water divide. *S*, sagged area with swamps developed in 1951 on the downthrown side of the Chihshang Fault. Rectangular frame: location of area mapped on right. (b) Topography of the Chihshang Fault area. Elevations in metres (isocontour interval: 5 m). Streams shown as dashed lines. *S*, sagged area with swamps (compare with (a)). Survey sites numbered 1, 2 and 3 (circled). See also Fig. 2.

studies near Chihshang, followed a period of uplift. The development of a major water divide along the Longitudinal Valley at Chihshang, partly tectonic in origin, is probably related to the late Quaternary compressional deformation of the crust which was concentrated in this area.

In more detail, the presence of topographic anomalies, such as for the elliptic sagged area with swamps on the downthrown side of the major fault scarp between Tapo and Chihshang (Fig. 3), highlights the recent deformation along the fault zone. Analyses of topographic maps, satellite imagery and aerial photographs revealed these features (Lee, 1994). This particular morphology is consistent with the results of levelling studies, which revealed a vertical relative displacement of about 3 cm/yr across the Chihshang Fault.

The active fault trace generally coincides with

the major reverse fault between the Pliocene Lichi Mélange (on the eastern, upthrust side) and the Quaternary alluvions of the Longitudinal Valley (Fig. 2). The Chihshang Fault also follows, and in some areas cut through, the edge of the Quaternary terraces along the eastern side of the Longitudinal Valley.

3. Kinematic analysis of active faulting: methods and results

The morphological analysis of active fault traces in Taiwan is more difficult than in desert areas, because of the humid tropical climatic conditions and extensive human activity. High rainfalls and large erosion rates, quick changes in natural vegetation and agriculture as well as multiple destruction and construction activities rapidly destroy active fault traces and modify outcrops. As a consequence, the local topography is of interest in a qualitative approach but generally brings little in terms of quantitative analysis of the deformation. For these reasons, we could not use the seismotectonic techniques commonly involved in desertic regions, but we took advantage of the presence of artificial features in this populated area.

Fractures affecting constructions above the Earth's surface (buildings and bridges) may be useful for finding the location of active fault traces, but fail to provide reliable records of deformation. They were not used in this study. Massive concrete walls, partly beneath the ground surface, are present along roads and water channels across the Chihshang Fault. They were used as bench-marks in order to quantify the fault displacement. Because of their strong coupling with the surficial terranes, they provide reliable local records of displacement. However, we ignored several sites where slope instability played an obvious or suspected role.

Along the Chihshang Fault, four sites finally matched severe requirements and allowed quantification of fault offsets. The three best sites are discussed in this paper. They are located in and between the villages of Tapo and Chinyuan, respectively east and southeast of Chihshang (Fig. 3b). At these sites, massive concrete walls were present: (1) a NNW–SSE-trending wall, facing the west and approximately 90 m long, along the entrance road of Tapo; (2) a concrete channel trending WNW–ESE, about 4 m wide and more than 100 m long, with two parallel walls, the most interesting segment being just west of the road from Tapo to Chinyuan; (3) another concrete channel, wider and longer (several hundred metres), with a NNW–SSE rectilinear segment forming the northeast limit of the Chinyuan village.

Our observations have been carried out since several years at four sites. Table 1 summarizes our observations and measurements since 1982, carried out on an annual basis since 1990. Systematic quantification of continuing displacement started in 1990 at Tapo, in 1991 at Chinyuan, and in 1992 in the site between Tapo and Chinyuan (Table 2). Our survey was interrupted in 1994 at the first two sites, because the damaged concrete structures were destroyed prior to reconstruction. Our data allow description of the deformation for a period of five years at Tapo (1990–1994), four years at Chinyuan (1991–1994) and three years in the third site (1992–1994). They include annual measurements of total fault displacements and determinations of motion vectors in terms of trends, plunges and amplitudes (Table 2). Concerning earlier periods, enquiries were done concerning the ages of wall construction at the three sites, in addition to our qualitative observations of initial fracturing; for these determinations, the accuracy is often less than one year. We thus obtained average velocity estimates since wall construction and fracturing, based on quantification of total deformation. Since 1992, more precise techniques have been used than before. New surveys were based on measurements of spacings of water drainage pipes in the walls (Table 3) and of lengths within nail networks (Table 4). The most accurate results were obtained in 1992–1993.

3.1. The Tapo access road: fault displacement vs. time

This site, mentioned first by Barrier and Chu (1984), was repeatedly surveyed (Chu et al., 1994) despite wall reconstruction (Table 1). In 1982, a well-developed reverse fault was observed in the wall along the road (Fig. 4a). The damaged wall was destroyed and rebuilt in 1984. New en-échelon fractures were observable in 1986 (Fig. 4b), indicating continuing reverse faulting. Our surveys from 1990 to 1994 showed increasing NNW–SSE shortening (Tables 2–4; Fig. 6). Increasing reverse slip on the

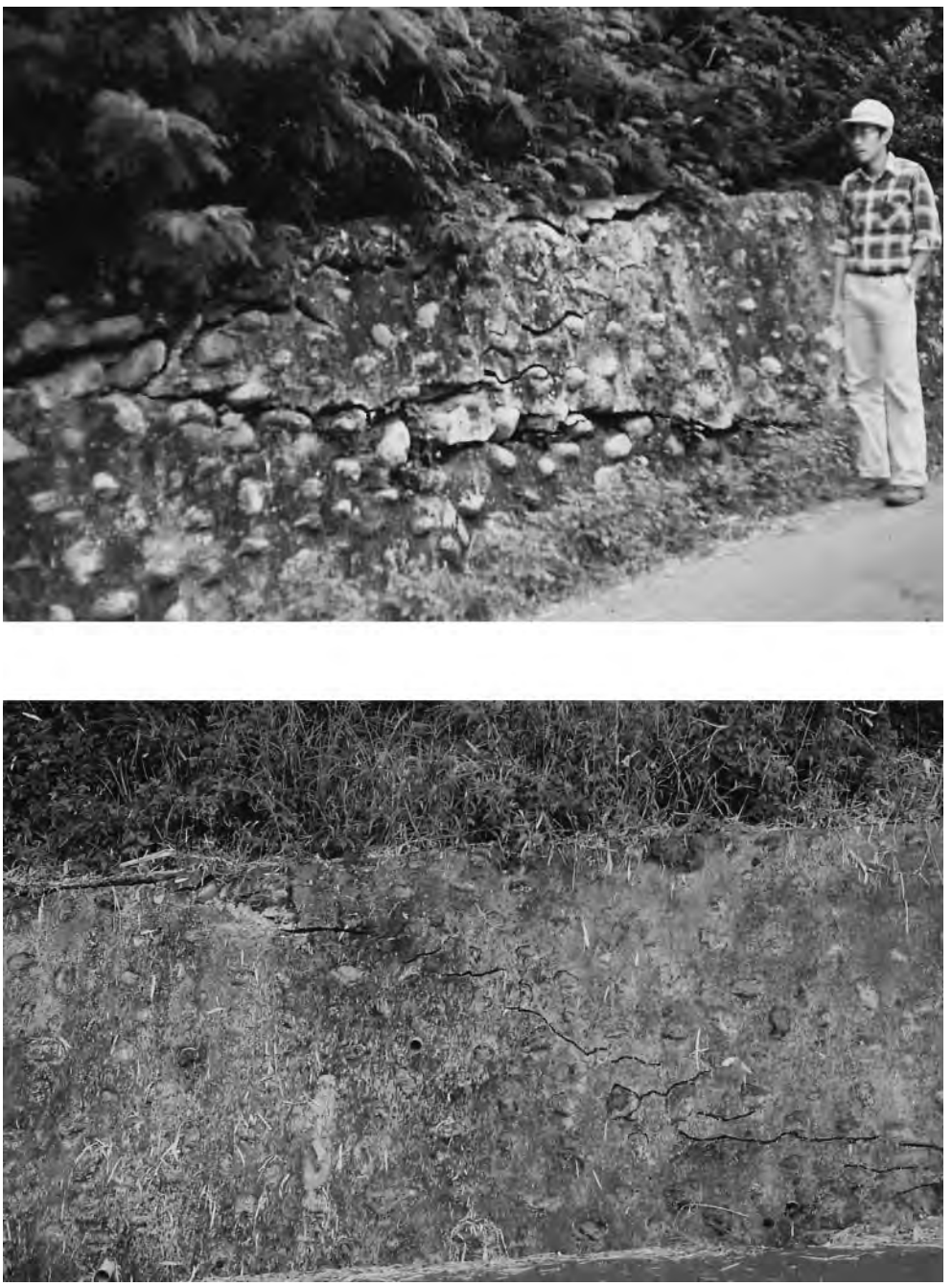

Fig. 4. The evolution of the Chihshang Fault until 1986, as recorded by two walls successively built across the active fault scarp, at the southwestern entrance of Tapo Village (location in Figs. 2 and 3b). Wall strikes NNW–SSE and faces west. See also Tables 1 and 2. Above (a): the faulted wall in 1982 (observation on 19-12-1982, ref. 188). Date of wall construction unknown. Scale: Chu Hao-Tsu. Below (b): same location, en-échelon fractures indicating ongoing reverse shear in new, higher wall (observation on 21-11-1986, ref. 637). Date of construction of new wall: early 1984. This fault is the upper fault of Tables 1–6 and Fig. 6. Wall height: 1.8–1.85 m. SSE on right.

Table 1
Summary of construction events, main observations and displacement data collection at the three main sites along the active Chihshang Fault, period 1982–1995 (dates given with day and month)

Year	Date	Tapo entrance road	Date	Tapo–Chinyuan channel	Date	Chinyuan channel
1982	09-12	Reverse fault observed in old wall. Fault strikes N23ºE. No displacement datum.				
1984		New wall built in early 1984.				Wall built in 1984–1985.
1986	21-11	New en-échelon fractures indicating reverse faulting.				
1988						Few fractures observed. Strike: N18ºE.
1990	19-01	New, lower fault 9.5 m appeared in 1989 north of first fault. Displacement data on both faults.		Channel built in 1987–1990.		
1991	27-01	Displacement data, upper and lower faults.		Fractures striking N165ºE.	27-01	Displacement data, upper and middle faults; lower fault poorly developed. Movement continuing on upper fault since June 1988.
1992	23-01	Displacement data, upper and lower faults. First nail network.	24-01	Displacement data, northern and southern sides. First nail network.	24-01	Displacement data, upper and middle faults. Channel bottom rebuilt. First nail network, upper fault.
1993	13-02	Displacement data, upper and lower faults. First data on 1992 nail network. Larger nail network installation.	14-02	Displacement data, northern and southern sides. First data on 1992 nail network.	15-02	Displacement data, upper and middle faults. Lower fault develops. First data on 1992 nail network. Larger nail network installation.
1994	30-01	Displacement data, upper and lower faults. New data on 1992 nail network.	30-01	Displacement data, northern and southern sides. New data on 1992 nail network. Larger nail network installation.	31-01	Displacement data, upper and middle faults. Lower fault develops. New data on 1992 nail network. New nail network, middle fault.
1995	14-02	Wall and network destroyed.	14-02	Channel and networks destroyed.	14-02	Survey continuing.

same fault is illustrated by the three views of the same place, in 1986 (Fig. 4b), 1990 (Fig. 5a) and 1992 (Fig. 5b). In 1990, a new, lower reverse fault developed 9.5 m west of the old one. Each of these faults was consequently surveyed during the later period (Fig. 6). The increasing contribution of the lower fault to the total shortening is illustrated by views in 1990 and 1992 (Fig. 7). In 1990, the upper fault was well-developed (Fig. 7a), whereas the upper fault had just appeared (Fig. 7b). In 1992, both these faults were well-developed (Fig. 7c), and most of the shortening was occurring on the lower fault (Table 2 and Fig. 6). Finally, the wall was rebuilt in 1994, so that our survey was interrupted.

Our earliest data collection was based on the observation and measurement on pre-existing benchmarks displaced along the faults (stones, pipes, wall crest and zig-zag patterns on fracture rims). The best data were obtained from the displacement of stones along the fault (relative to their imprints on the opposite side), principally near the base of the wall and at places where the fault is unique (rather than across multiple, nearly parallel fractures). At Tapo, such collection of total displacement data in terms of orientation and length was done yearly from 1990 to 1993 (Table 2). It was interrupted later because of increasing damage and auxiliary fracture development along the faults. The accuracy of these measure-

Table 2
Summary of cumulative displacement data (in cm), with measured trends and plunges of corresponding displacement vectors (in degrees, trends given as azimuths) at the three main sites along the active Chihshang Fault, period 1984–1995

Year	Date	Tapo entrance road	Date	Tapo–Chinyuan channel	Date	Chinyuan channel
1982	9-12	Trend of displ. vector: 147 ± 10 (1).		Channel built in 1987–1990.		
1990	19-01	Upper fault: 8.0 ± 0.6 (2); displ. vector: 155 ± 10, 35 ± 10 (1). Lower fault: 1.2 ± 0.4 (3).				
1991	27-01	Upper fault: 9.6 ± 0.4, (4); displ. vector: 163 ± 4, 35 ± 4 (2). Lower fault: 3.6 ± 0.4 (5); displ. vector: 158 ± 12, 30 ± 10 (1).			27-01	Upper fault: 4.0 ± 0.4 (6); displ. vector: 158 ± 8, 26 ± 3 (2). Middle fault: 1.3 ± 1.0 (5).
1992	23-01	Upper fault: 10.2 ± 0.4 (4); displ. vector: 163 ± 8, 30 ± 6 (3). Lower fault: 6.0 ± 0.4, (2); displ. vector: 150 ± 2, 42 ± 6 (4).	24-01	South side: 2.4 ± 0.3 (1). North side: 2.0 ± 0.2 (2); displ. vector: 308 ± 3, 42 ± 5 (1).	24-01	Upper fault: 5.4 ± 0.2 (4); displ. vector: 156 ± 4, 26 ± 5 (1).
1993	13-02	Upper fault: 11.4 ± 0.2, (3); displ. vector: 157 ± 2, 29 ± 4 (2). Lower fault: 8.7 ± 0.4, (2); displ. vector: 148 ± 8, 42 ± 2 (2).	14-02	South side: 5.9 ± 0.2 (1); displ. vector: 285 ± 5, 51 ± 6 (1). North side: 5.6 ± 0.5 (1); displ. vector: 305 ± 5, 39 ± 5 (1).	15-02	Upper fault: 6.4 ± 0.3 (3); displ. vector: 156 ± 2, 26 ± 5 (2).
1994			30-01	South side: 8.6 ± 0.2 (1); disp. vector: 283 ± 5, 46 ± 6 (1). North side: 6.9 ± 0.5 (2); displ. vector: 321 ± 5, 37 ± 5 (2).	31-01	Upper fault: 7.1 ± 0.2 (2); displ. vector: 154 ± 4, 30 ± 5 (3).

Numbers between parentheses are numbers of data. Total displacement refers to wall construction dates. Displacement vectors describe motion of the lower block relative to the upper one.

Table 3
Summary of displacement data for each year (in cm), measured along nearly horizontal lines of pipes in walls at three main sites along the active Chihshang Fault, period 1982–1994

Year	Date	Tapo entrance road	Date	Tapo–Chinyuan channel	Date	Chinyuan channel
1992	23-01	First measurement. Upper and lower faults: 1 line of 10 pipes, 26 m long; orientation: 346 ± 5, 6 ± 1.	24-01	First measurement. South side: line of 5 pipes, 10 m long; orientation: 300 ± 2, 2 ± 1. North side: line of 8 pipes, 17 m long; orientation: 299 ± 2, 2 ± 1.	24-01	First measurement. Upper fault: line of 12 pipes, 20 m long; orientation: 338 ± 2, 3 ± 1. Middle fault: line of 9 pipes, 17 m long; orientation: 335 ± 3, 3 ± 1.
1993	13-02	Upper fault: shortening 1.0 ± 0.2 since 23-01-92. Lower fault: shortening 2.95 ± 0.3 since 23-01-92.	14-02	South side: shortening 3.2 ± 0.4 since 24-01-92. North side: shortening 3.2 ± 0.3 since 24-01-92.	15-02	Upper fault: shortening 0.7 ± 0.4 since 24-01-92.
1994	30-01	Upper fault: shortening 0.5 ± 0.2 since 13-02-93. Lower fault: shortening 1.3 ± 0.3 since 13-02-93.	30-01	South side: shortening 1.1 ± 0.4 since 14-02-93. North side: shortening 1.55 ± 0.3 since 14-02-93.	31-01	Upper fault: shortening 0.85 ± 0.3 since 15-02-93.

Average trends (azimuths) and plunges of lines (degrees) indicated with first measurement lines.

Table 4
Summary of horizontal shortening data for each year (in cm), measured in nail networks in walls at the three main sites along the active Chihshang Fault, period 1982–1994

Year	Date	Tapo entrance road	Date	Tapo–Chinyuan channel	Date	Chinyuan channel
1992	24-01	Network installation, 17 points, 26 m long; orientation: 253 ± 4, 67 ± 3. Upper and lower faults.	24-01	Network installation. South side: 7 points, 5 m long; orientation: 032 ± 2, 76 ± 2. North side: 5 points, 7 m long; orientation: 211 ± 2, 75 ± 2.	24-01	Network installation. Upper fault: 10 points, 10 m long; orientation: 247 ± 2, 70 ± 2. Middle fault: 4 points, 5 m long; orientation: 245 ± 3, 69 ± 3.
1993	13-02	Upper fault: shortening 1.95 ± 0.2 since 24-01-92. Lower fault: shortening 2.15 ± 0.3 since 24-01-92. Network increased (46 points).	14-02	South side: shortening 2.8 ± 0.2 since 24-01-92. North side: shortening 3.0 ± 0.2 since 24-01-92. Shortening trend: 115 ± 3.	15-02	Upper fault: shortening 1.15 ± 0.2 since 24-01-92. Middle fault: shortening 1.05 ± 0.2 since 24-01-92. Network increased (11 points).
1994	30-01	Upper fault: shortening 0.4 ± 0.1 since 13-02-93. Lower fault: shortening 1.0 ± 0.2 since 13-02-93.	30-01	South side: shortening 1.4 ± 0.2 since 14-02-93. North side: shortening 1.2 ± 0.2 since 14-02-93. Shortening trend: 122 ± 4. Networks increased (29 points).	31-01	Upper fault: shortening 1.1 ± 0.2 since 15-02-93. Middle fault: shortening 0.5 ± 0.2 since 15-02-93.

Average strikes and dips of networks (in degrees, strikes given as azimuths) indicated with first network installation lines.

ments of total fault offset since wall construction and fracturing averages 0.4 cm (Table 2).

During the period 1992–1994, more accurate and systematic displacement data collection in this wall was carried out by using (1) pre-existing water drainage pipes, and (2) a network of nails that we installed in 1992. Such data collection used better bench-marks, was submitted to cross-checking procedures and was not affected by local damage along faults. The accuracy was thus better and averaged 0.2–0.3 cm (Tables 3 and 4). As a counterpart, such measurements of incremental deformation by essence did not provide estimates of total displacement since wall construction and fracturing. The first displacement data were obtained in 1993 (both the nail network installation and the first survey on line of pipes were carried out in 1992). Because of wall destruction in 1994, they were only available for two years.

It is worthwhile to compare these two groups of techniques. In addition to differences in reliability, accuracy and time scale (cumulative vs. incremental) of these contrasting data collecting modes, there is a major geometrical difference in terms of orientation. Measurements of displacement vectors in terms of trend, plunge and length are possible in the first case (Table 2). In contrast, measurements collected along lines of pipes only provide components of displacement along lines (Table 3), and those made within nail networks provide access to the components of deformation within planes (Table 4). Because the height of the nail network was small, the vertical components of deformation were subject to large uncertainties, so that in practice this analysis principally yielded estimates of nearly horizontal displacement parallel to wall strike, such as for pipes. The accuracy and reliability were however better with nails, resulting not only from better definition of nodes but also from internal geometrical constraints within the multiple triangles of the network.

An important difference between these two groups of techniques lies in the size of the domain surveyed: the data shown in Table 3 are local (along fractures) and do not include the effects of possible deformation within the blocks on both sides of each fault. In contrast, the length data shown in Tables 3 and 4 describe and constrain the whole deformation along the wall, and thus have the capacity to allow detection of deformation without macroscopic fracturing. However, all measurements within nail networks along the Chihshang Fault showed that shear is strictly located along the faults, the deforma-

Fig. 5. The 1990–1992 evolution of the Chihshang Fault recorded by a wall across the active reverse fault scarp, at the southwestern entrance of Tapo village (location in Figs. 2 and 3b). Same place and wall as for Fig. 4b (built in early 1984, striking NNW–SSE, facing west and 1.8–1.85 m high). SSE on right. Note increasing damage along reverse fault. Between (a) and (b), horizontal shortening of 2.2 cm has occurred, nearly parallel to wall strike. See also Tables 1 and 2 (the fault is the upper fault). Above (a): faulted wall in 1990 (observation on 19-01-1990, ref. 1532). Scale: Lee Teh-Quei. Below (b): same faulted wall in 1992 (observation on 23-01-1992, ref. 2137). Scale: Chu Hao-Tsu.

tion of the wall being negligible elsewhere (between the faults, the differences in lengths for successive surveys remained smaller than the uncertainties). Similar amounts of shortening were thus computed with three independent data collecting modes for 1992, 1993 and 1994 (compare Tables 2–4).

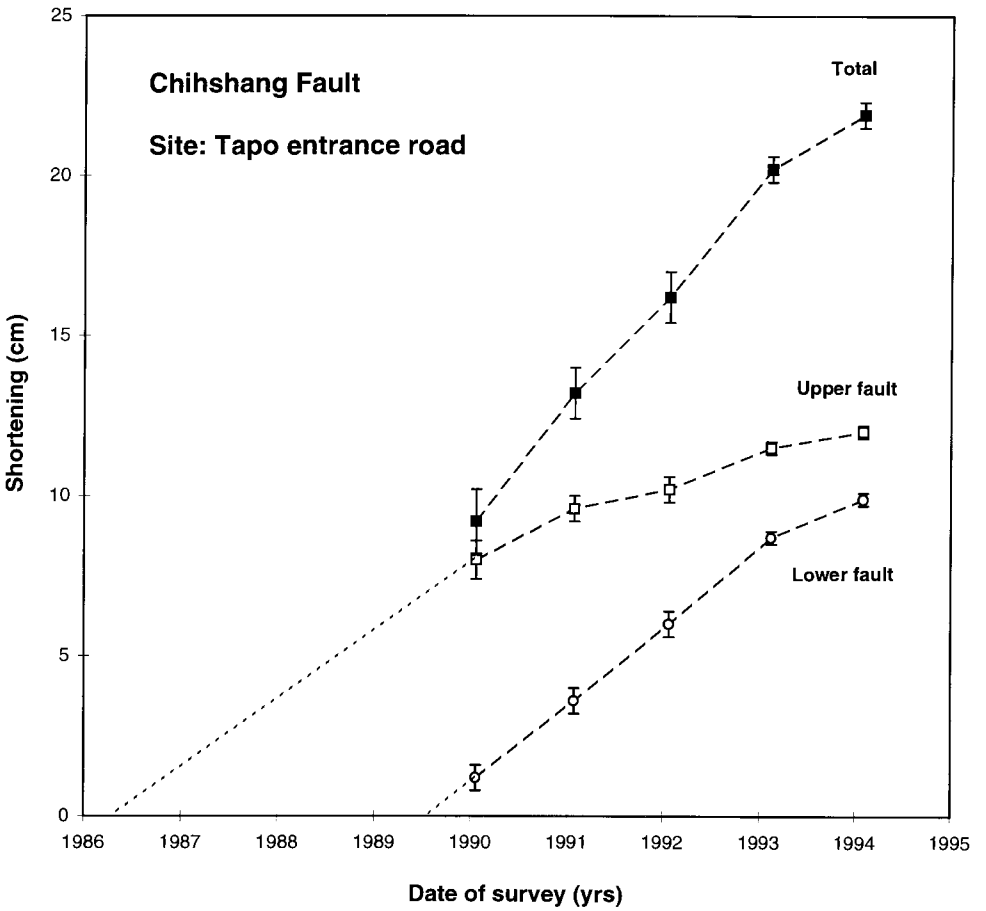

Fig. 6. Horizontal shortening (ordinates, in cm) versus time across the Chihshang active fault scarp, site of the Tapo entrance road. See also Tables 1–5 and discussion in text. Open dots and squares: data from the lower and upper faults, respectively. Black squares: total shortening. Error bars shown. Dotted lines: average shortening since first appearance of fractures in the wall.

In these geometrical reconstitutions, particular attention was paid to possible rotations or flexuring affecting the walls studied. Both the surveys of wall crests (which remained rectilinear parallel segments between faults) and the analysis of pipe alignments and nail networks revealed that the wall cracking was not due to flexuring processes and that rotations were absent or negligible. This observation was done at Tapo as well as at the other two sites.

We conclude that despite the differences listed above, these three sources of data are complementary and should be combined. This is done in Table 5 and Fig. 6, where the cumulative displacements are listed and illustrated, and in Table 6 which summarizes the corresponding yearly rates of shortening. At Tapo, it is obvious that within the range of uncertainties the increase in total shortening was nearly linear during the period 1990–1993. It slightly diminished in 1994 (see Fig. 6). Furthermore, based on total shortening estimates and knowing that wall fracturing began in 1986, the average rates of shortening computed for the 1986–1989 and 1990–1994 periods are equivalent. The final shortening affecting the wall built in 1984 is 21.9 cm for about 8 years (1986–1994), that is 2.7 cm/yr (Fig. 6). Until 1989, the whole shortening occurred across a single fault (Figs. 4 and 5), whereas starting in 1989 the new, lower fault played an increasing role (Fig. 7) and finally accounted for most of the movement while the previous, upper fault became less and less active (Fig. 6).

Table 5
Cumulative displacements at the three main sites along the active Chihshang Fault, period 1984–1994, based on compilation of all results from Table 1Table 2Table 3Table 4

Year	Date	Tapo entrance road	Date	Tapo–Chinyuan channel	Date	Chinyuan channel
1986	21-11	Fracturing has begun in wall built in early 1984.				
1988						Fracturing begins in walls built in 1984–1985.
1990	19-01	Upper fault: 8.0 ± 0.6. Lower fault: 1.2 ± 0.4. Total: 9.2 ± 1.0.		Fracturing begins in walls built in 1987–1991.		
1991	27-01	Upper fault: 9.6 ± 0.4. Lower fault: 3.6 ± 0.4. Total: 13.2 ± 0.8.			27-01	Upper fault: 4.0 ± 0.4. Middle fault: 1.3 ± 1.0. Total: 5.3 ± 1.4.
1992	23-01	Upper fault: 10.2 ± 0.4. Lower fault: 6.0 ± 0.4. Total: 16.2 ± 0.8.	24-01	2.4 ± 0.3.	24-01	Upper fault: 5.4 ± 0.2. Middle fault: 2.4 ± 1.0. Total: 7.8 ± 1.2.
1993	13-02	Upper fault: 11.5 ± 0.2. Lower fault: 8.7 ± 0.2. Total: 20.2 ± 0.4.	14-02	5.8 ± 0.3.	15-02	Upper fault: 6.4 ± 0.2. Middle fault: 3.5 ± 1.0. Total: 9.9 ± 1.2.
1994	30-01	Upper fault: 12.0 ± 0.2. Lower fault: 9.9 ± 0.2. Total: 21.9 ± 0.4.	30-01	7.5 ± 0.3.	31-01	Upper fault: 7.2 ± 0.2. Middle fault: 4.2 ± 1.0. Total: 11.4 ± 1.2.

Uncertainty estimates based on combination of data of various numbers and qualities (see discussion in text). For middle fault of Chinyuan channel, information collected in 1995 was used to determine previous offsets.

In terms of orientations, within the Tapo road wall striking NNW–SSE, the fifteen motion vectors measured in 1990–1994 trend N156ºE and plunge 36ºS on average (Table 2), whereas the fault trace strikes N23ºE. The wall of the Tapo entrance road is thus oblique to the fault trend at an angle of about 45º, which may influence the behaviour of the broken wall. On the other hand, the obliquity of the NNW–SSE motion vector trends relative to the NNE–SSW fault strike highlights the role of oblique slip, both reverse and left-lateral, along the Chihshang Fault. It is however indispensable to examine sites with simpler geometrical relationships between walls and fault traces (next subsection).

3.2. The Tapo–Chinyuan water channel: fault displacement orientation and velocity

Between Tapo and Chinyuan, active faulting affected a concrete water channel, 4.3 m wide, which trends WNW–ESE in a flat area near the fault scarp (a location precluding the development of slope-related features). This channel was built in 1987–-1990 and N–S fractures were observed as soon as 1990–1991 (Table 1). An east-vergent fault developed in the concrete walls, as the surface expression of the main west-vergent reverse fault. Two views of this fault, taken in 1992 and 1994, are shown in Fig. 8. The channel was destroyed in 1994.

Fig. 7. Reverse faults in 1990 and 1994 at the southwestern entrance of Tapo village, after development of a new, lower reverse fault in 1989. Same wall as for Fig. 4b and Fig. 5 (built in 1984, striking NNW–SSE, facing west and 1.8–1.85 m high). SSE on right. Above (a): upper fault in 1990 (observation on 27-01-1991, ref. 1869). Centre (b): lower fault in 1990 (observation on 27-01-1991, ref. 1859). Below (c): both these faults in 1994 (observation on 30-01-1994, ref. 2782). From 1990 to 1994, horizontal shortenings of 4 cm and 8.7 cm occurred on upper and lower faults, respectively, nearly parallel to wall strike. See also Tables 1 and 5.

Table 6
Average velocities of fault slips at three main sites along the Chihshang Fault, period 1984–1994, in cm/yr, for periods of about one year (or longer where specified; details in other tables)

Years	Tapo entrance road	Tapo–Chinyuan channel	Chinyuan channel
Before January 1990	Upper fault: 2.0 (4 years). Lower fault: 0.6 (2 years). Total: 2.3 (4 years).		
1990	Upper fault: 1.6. Lower fault: 2.4. Total: 4.0.		Upper fault: 1.3 (3 years). Middle fault: 0.5 (3 years). Total: 1.8.
1991	Upper fault: 0.6. Lower fault: 2.4. Total: 3.0.	1.2 (2 years).	Upper fault: 1.4. Middle fault: 0.9. Total: 2.5.
1992	Upper fault: 1.3. Lower fault: 2.7. Total: 4.0.	3.4.	Upper fault: 1.0. Middle fault: 1.1. Total: 2.1.
1993	Upper fault: 0.5. Lower fault: 1.2. Total: 1.7.	1.7.	Upper fault: 0.8. Middle fault: 0.7. Total: 1.5.

Data collection was made in 1992 for total displacement since channel construction and fracturing, and in 1993 and 1994 with the three techniques described in the previous subsection (measurements on pre-existing bench-marks, aligned drainage pipes and nail networks). A summary of data is given in Tables 2–4. The results of our kinematic analysis in this site are summarized in Table 5 and Fig. 9 for cumulative displacements, and in Table 6 for average velocities. Despite a smaller number of surveys (because of later construction), the results are compatible with a rather stable velocity of horizontal shortening, that is 2.1 cm /yr, resulting in a total displacement of 7.5 cm in about 3.5 years (1990–1994). Considering the error bars (Fig. 9), variations may be not significant.

The particular interest of this site lies first in the WNW–ESE direction of the concrete channel, which is almost perpendicular to the NNE–WSW active fault trace, and second on the presence of the two channel walls forming a symmetrical pattern. This geometrical distribution allowed better estimation of the orientation of fault motion vectors. Six motion vectors could be measured from 1992 to 1994, as Table 2 shows. The plunges (39° on the northern side, 48° on the southern one) are compatible considering the angular uncertainty of about 5°, indicating an average value of 42°. In contrast, the trends significantly differ depending on the channel side. The average values are N134°E in the northern wall and N104°E in the southern one: a difference larger than the azimuthal uncertainty (less than 5°). Relative to the N121°E trend of the channel, the trends of motion vectors on the northern and southern sides make angles of 13° clockwise and 17° counter-clockwise, respectively.

This distribution is related to a minor component of displacement of the upper block towards the free axis of the channel, as a result of the pressure exerted by the adjacent terranes on the fractured walls. Despite the rigidity of buried concrete walls, the determination of fault motion vectors is slightly vitiated by the deviatoric effects of gravity (because of the absence of earth on one side of a wall). Considering both the intrinsic symmetry of the channel and its orientation nearly perpendicular to the active fault trace, we conclude that the average between the trends of motion vectors reconstructed independently on the two sides reliably describes the actual trend of the actual fault motion vector for the period 1991–1994, that is, N119°E.

This comparison between the two rims of the Tapo–Chinyuan channel suggests that where fault movements were recorded in asymmetrical features,

Fig. 8. Example of wall affected by active reverse fault, at the site between Tapo and Chinyuan (channel built in 1987–1990). Southern side of channel (wall striking WNW–ESE, facing north and 1.5 m high). WNW on right. Location in Figs. 2 and 3. Above (a): fault in 1992 (observation on 24-01-1992, ref. 2199). Below (b): fault in 1994 (observation on 30-01-1994, ref. 2828). From 1992 to 1994, horizontal shortening of 5.1 cm occurred, nearly parallel to wall strike. See also Tables 1 and 5.

or features trending obliquely to fault traces (which was the case at Tapo), the results obtained in terms of motion vector orientation should be considered with caution: deviations as large as 15° may occur because of lateral ground pressure. However, these deviations occur in such a way that the additional component of motion of the upper block relative to the lower is directed towards the free side of the wall. They played a little role in the first site where motion vectors trend nearly parallel to wall strike.

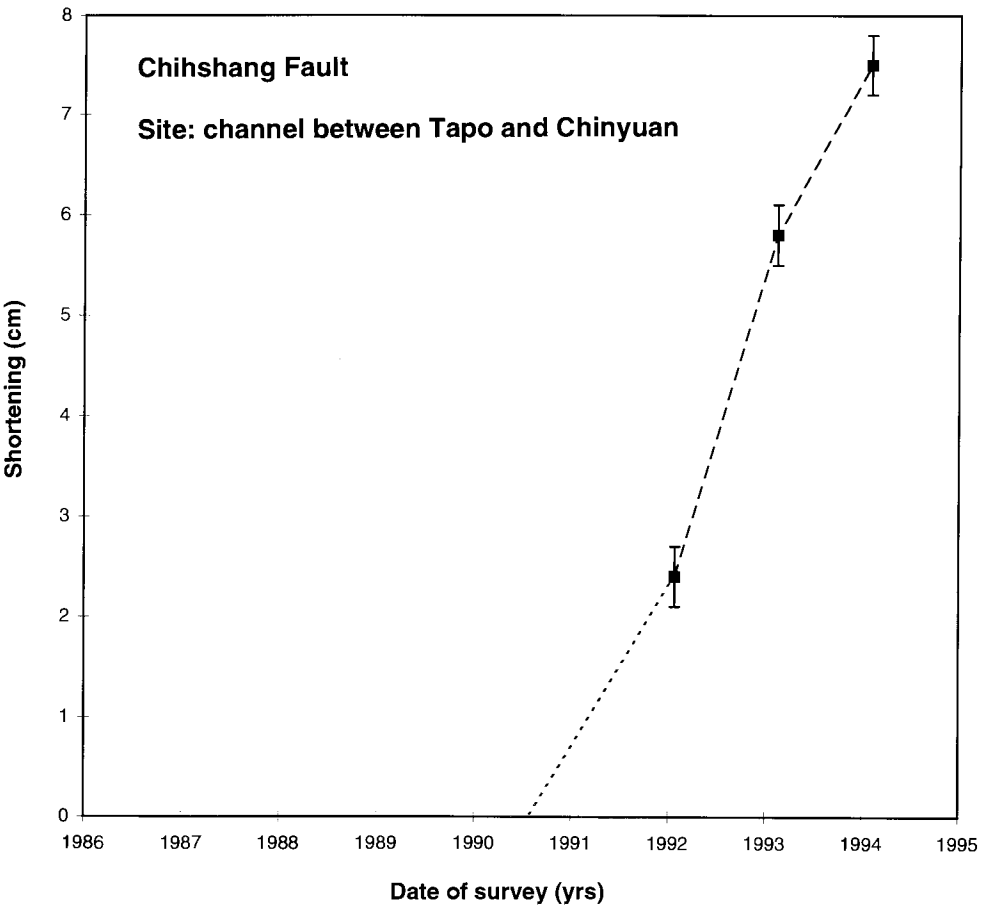

Fig. 9. Horizontal shortening (ordinates, in cm) versus time across the Chihshang active fault scarp, site of the water channel between Tapo and Chinyuan. See also Tables 1–5 and discussion in text. Error bars shown. Dotted lines: average shortening since first appearance of faults in the wall.

Both the determinations of motion vector trends, N156ºE along the Tapo road and N119ºE in the Tapo–Chinyuan channel, should thus be considered valid.

3.3. The Chinyuan water channel: multiple faults across a fault zone

Numerous evidences of active faulting were found in the Chinyuan village, such as for offsets affecting houses and farms. The most reliable displacement estimates were obtained in a NNW–SSE-trending water channel, where two main fracture zones with a horizontal spacing of about 40 m developed (upper and middle faults in Tables 1–6). Fractures with little displacement were also observed in 1992 at a distance of about 200 m downstream, suggesting that a third, lower fault develops. The Chinyuan channel site thus illustrates fracturing and faulting along several branches of the Chihshang Fault.

Fig. 10. Progressive shear from 1991 to 1995 on reverse fault in the wall of the Chinyuan channel site, as illustrated by increasing deformation of the same water drainage pipe in the fault cutting the wall. Wall strikes NNW–SSE and faces west, pipes are nearly horizontal and perpendicular to wall strike. Intact pipe diameter is 6 cm. SSE on right. Above, on left (a): pipe in 1991 (observation on 27-01-1991, ref. 1828). Above, on right (b): pipe in 1992 (observation on 24-01-1992, ref. 2203). Below, on left (c): pipe in 1994 (observation on 31-01-1994, ref. 2856). Below, on right (d): fault in 1995 (observation on 14-02-1995, ref. 3169). From 1991 to 1995, horizontal slip of about 7 cm occurred, nearly parallel to wall strike.

Across the upper fault, continuing displacement is illustrated not only by bench-mark offsets, but also by the increasing deformation of water drainage pipes such as in Fig. 10, where a single pipe is shown at different stages of shear deformation (Fig. 10a, b, c and d, in 1991, 1992, 1994 and 1995, respectively). The main fracture locally followed a line of pipes in the wall, because series of parallel pipes crossing the wall created a zone of weakness exploited by fracture development and propagation. Two extreme stages of shear deformation affecting pipes at other sites in 1994 are shown in Fig. 11: incipient shear along the upper fault at Tapo, and complete crushing of a pipe in the fault at the site between Tapo and Chinyuan.

The concrete channel walls of the Chihshang channel were built in 1984–1985; fractures with NNE–SSW strikes were observed in 1988 but may have developed earlier. The following history resembles that of the Tapo entrance road, with total displacement data being collected from 1991 to 1994 (Table 2) and accurate surveys starting in 1992 (Tables 3 and 4). The techniques were identical to those used in Tapo. The results are summarized in Table 5 and Fig. 12 for cumulative displacements, and in Table 6 for average velocities. Note that the middle fault includes two branches with a spacing of a few metres and crosses a sharp bend of the channel, so that because of complex deformation in curved walls the accuracy of length measurements was poor (Table 5) and no reliable orientation of motion vector was measured.

Concerning the upper fault at Chinyuan, the geometrical relationship between wall strike, fault strike and motion vector trend resembles that observed in Tapo (Tables 1 and 2). This highlights the origin of the general correspondence between wall strikes and motion vector trends (an intriguing coincidence at first sight). This correlation exists because at other sites, where walls strike perpendicular or oblique at large angles to motion vector trends, the deformation was so complicated (with multiple fracturing and rotation of wall segments) that reliable displacement data could not be collected. The sites which had the capacity to provide significant data, and were retained in this study, thus corresponded to special geometrical situations, with walls striking parallel, or oblique at small angles, to motion vectors trends.

Considering the orientations of motion vectors at Chinyuan, they resemble those observed at Tapo, with consistent average values: N155ºE for the trend and 27º for the plunge. Because in Chinyuan the geometrical relationships between wall, fault and motion are quite the same as in Tapo, the orientations listed in Table 2 for the upper fault should be considered acceptable. It is likely that for the middle fault the motion vector trends are similar.

The record of fault displacement obtained at Chinyuan (Fig. 12) is also interesting in that it illustrates the development of a new reverse fault zone (the middle fault) below the main one, at a larger distance (40 m downstream) than for Tapo. This middle fault probably appeared in late 1989 to early 1990. Incipient fracturing about 200 m downstream suggests an incipient stage for a third, lower fault. The estimates of the total motion at Chinyuan are vitiated by the poor record for the middle fault, despite excellent accuracy for the upper fault (Table 5 and Fig. 12). However, the results are compatible with a rather stable velocity of horizontal shortening, that is 1.9 cm /yr, resulting in a total displacement of 11.4 cm in about 6 years (1988–1994). As for the other sites, the velocity slightly decreased in 1993 (Fig. 12).

4. Kinematics of the Chihshang Fault

4.1. Local kinematics

The results of the displacement data collected in the three sites studied can be summarized as follows, keeping in mind the previous discussion of reliability and accuracy.

At Tapo, the horizontal shortening affecting the road wall built in early 1984 started in 1986 and was as large as 21.9 cm after about 8 years (1986–1994), with an average velocity of 2.7 cm/yr (Fig. 6). The average motion vector trended N156ºE and plunged 36ºS.

At Chinyuan, the horizontal shortening affecting the channel wall built in 1984–1985 started in 1988 and was as large as 11.4 cm after about 6 years (1988–1994), with an average velocity of 1.9 cm/yr (Fig. 12). The motion vector trended N155ºE and plunged 27ºS.

At the site between Tapo and Chinyuan, the

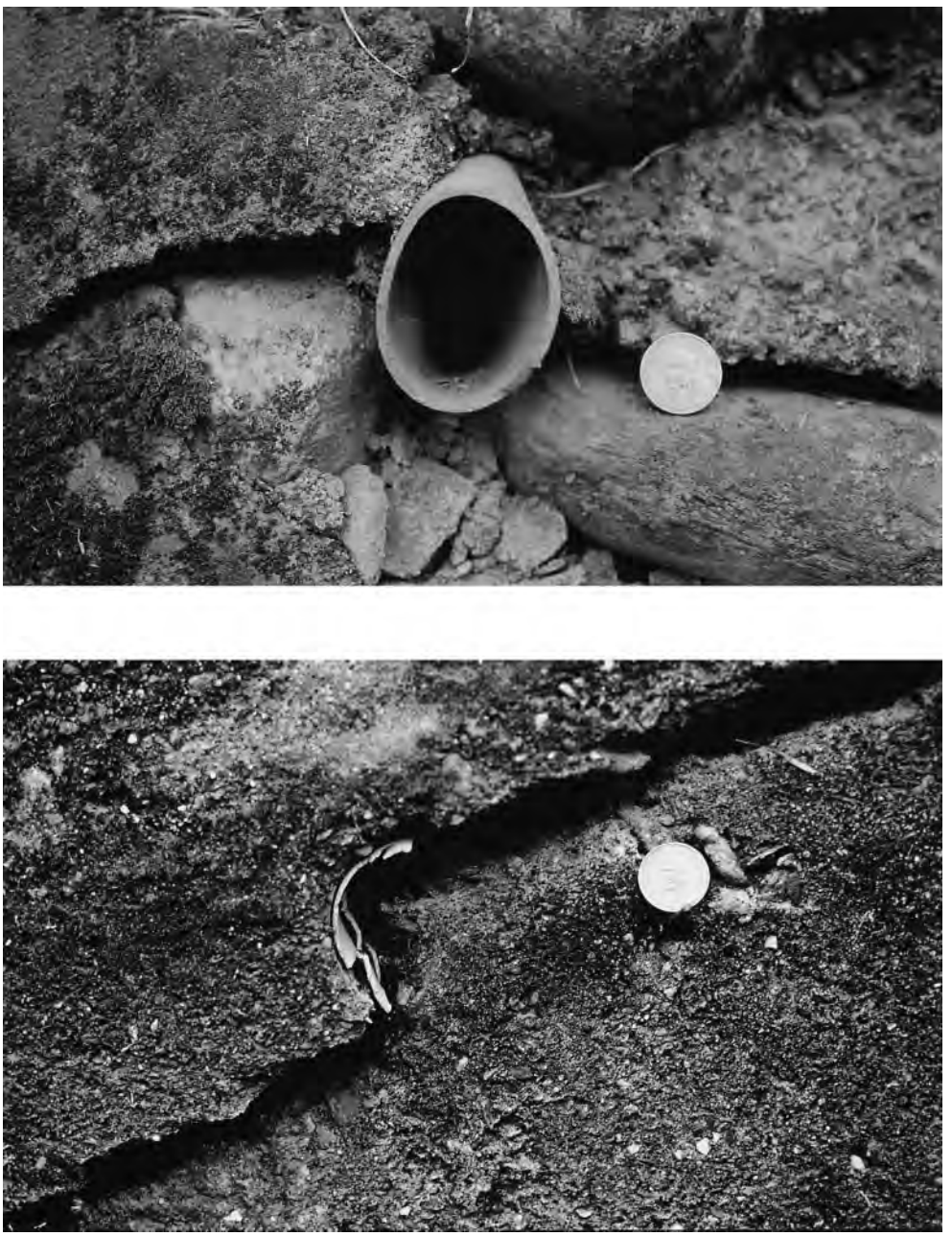

Fig. 11. Minor and major shear deformation affecting water drainage pipes in reverse faults. Compare with Fig. 10. Above (a): site of Tapo entrance road, upper fault (observation on 30-01-1994, ref. 2823). Below (b): site of Tapo–Chinyuan channel, southern side (observation on 30-01-1994, ref. 2842).

horizontal shortening affecting the channel built in 1987–1990 started in 1991 and was as large as 7.5 cm after about 3.5 years (1990–1994)), with an average velocity of 2.1 cm/yr (Fig. 9). The motion vector trended N119ºE and plunged 42ºW, which may reflect particular accommodation of fault slip related to strain release in front of the previous zone of maximum downwarping west of the Chihshang

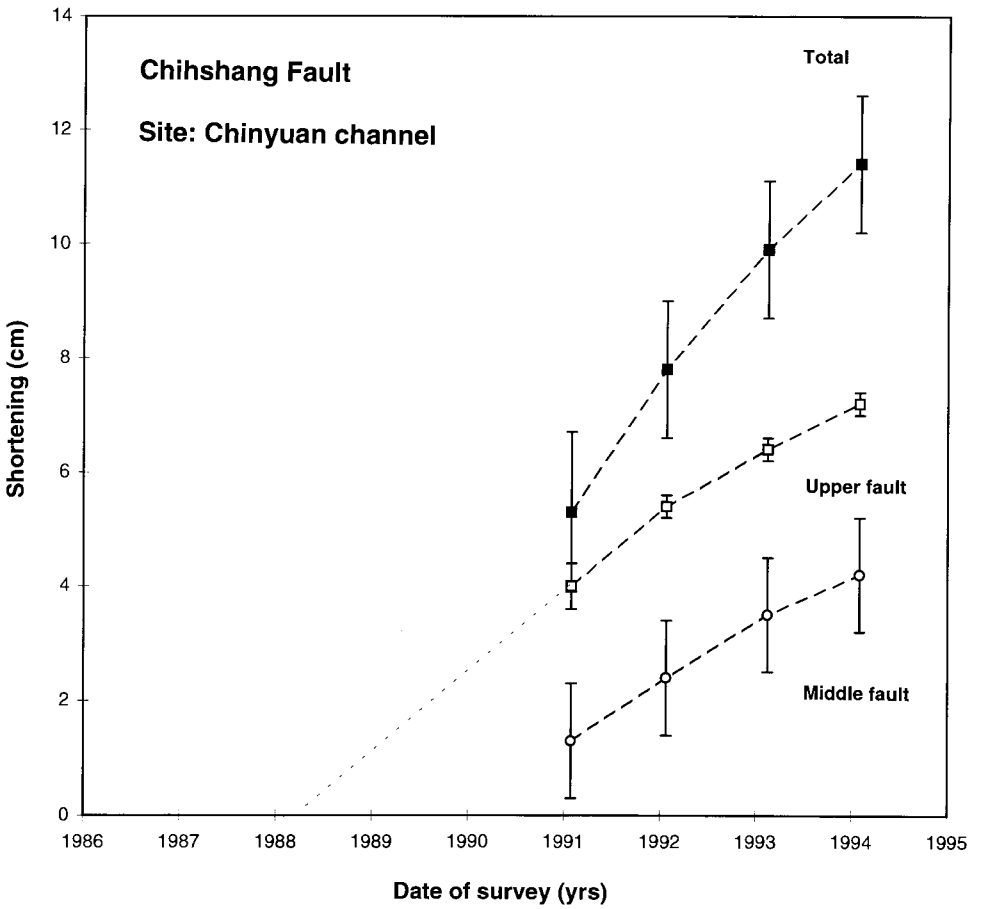

Fig. 12. Horizontal shortening (ordinates, in cm) versus time across the Chihshang active fault scarp, site of the water channel in Chinyuan. See also Tables 1–5 and discussion in text. Open dots and squares: data from the lower and upper faults, respectively. Black squares: total shortening. Error bars shown. Dotted line: average shortening since first appearance of faults in the wall.

zone (the 1951 sagged depression of Fig. 3). Because fractures in concrete walls typically behave as reverse faults with a component of vertical opening, their dips are of little interest, whereas the plunge of motion vectors reveals deeper fault geometry.

In terms of average velocities, the results obtained at the three sites studied are generally compatible and reveal a horizontal shortening of about 2.2 cm/yr across the Chihshang Fault. Furthermore, the annual amount of shortening is nearly constant in all sites, as illustrated by the approximately linear increase in total displacement (compare Figs. 6, 9 and 12). There are some variations, such as for a slight increase in velocity at Tapo, coinciding with the development in 1989–1990 of a new fault beneath the older one (a phenomenon that occurs at a wider scale at Chihshang). Such local variations, which may reflect variable distribution of strain between fault branches through time, should not be interpreted in terms of kinematic variations of the whole fault zone in the absence of independent evidences.

More interesting is the decreasing velocity consistently measured in 1993–1994 at the three sites (Figs. 6, 9 and 12). For a period of 11.5 months, the shortening was 1.7 cm at Tapo, 1.5 cm at Chinyuan and 1.7 in the intermediate site, indicating an average velocity of 1.7 cm/yr. This velocity is half of that measured for the twelve preceding months in the same sites (shortenings of 4 cm, 3.4 cm and 2.1 cm, respectively, i.e., an average velocity of 3.2

cm/yr) and three fourths of the average velocity of 2.2 cm/yr for longer periods (see Tables 5 and 6). Further studies should reveal whether this decrease in velocity continues or not. In the first case, this phenomenon would reveal a decreasing activity of the Chihshang Fault, suggesting that compressional strain is accumulating elsewhere. This would imply increasing earthquake risk along the Chihshang segment of the Longitudinal Valley.

In terms of motion vector trends, there is a significant difference between the results obtained at Tapo and Chinyuan (NNW–SSE convergence) and in the intermediate site (WNW–ESE convergence). Many evidences for active faulting during the last twelve years or more are concentrated within the 3-km-long Tapo–Chinyuan segment of the Chihshang Fault. The fault being oblique-slip (reverse-sinistral), it is not surprising that the ratio between strike-slip and reverse offsets varies along this segment, being larger near the tips (the sites at Tapo and Chinyuan) than between (the intermediate site). Within the range of uncertainties, the average trend of motion vectors better represents the actual behaviour of the fault. We conclude that the relative displacement occurs in a N143ºE (N37ºW) direction on average.

From a methodological point of view, we noticed that in the three sites incipient fracturing related to continuing fault motion did not develop immediately after wall construction but approximately two years later (Table 1). Because of various construction dates, this delay cannot be interpreted in terms of variations in fault kinematics. It is probably related to a period of increasing elasto-plastic strain within surrounding surficial terranes, prior to wall break which requires local shear stress higher than cohesion and friction in the concrete structure. This interpretation implies that prior to rupture, shortening took place with no or little fracturing in walls. Such compressive deformation occurred possibly within the wall (for a limited amount) and certainly within the ground (especially near wall tips).

According to this interpretation, after wall breaking, the shortening rate across a fault in a wall was slightly larger than the average shortening across the fault zone, until elasto-plastic strain was released and came back approximately to its previous level. In other words, the walls ‘stored’ deformation in the time after construction and before cracking. Accordingly, in order to obtain realistic estimates for fault kinematics, the average shortening velocity would be better calculated based on the wall construction date rather than on the first fracturing date (in order to eliminate the bias introduced by strain accumulation before wall breaking). In this respect, in Fig. 6, a straight line beginning in 1984 (wall construction) would better represent the deformation behaviour across the fault than the line based on initial fissuring in 1986.

Our data did not allow checking this hypothesis, which is supported by the relatively high values of shortening that we obtained (especially in Tapo), relative to those obtained at a larger scale in the Chihshang network (Yu and Liu, 1989). It is also quite significant that with a calculation of average shortening velocities based on wall construction dates, the largest value for the longest period is 2.2 cm/yr at Tapo (21.9 cm in ten years), which fits the value of shortening calculated within the Chihshang geodetic network discussed in the next subsection.

4.2. Comparisons with the results of geodetic surveys in the Longitudinal Valley

We compared the results of our local site surveys along the Chihshang active fault with the earlier results independently obtained based on geodetic surveys in the same region.

Three networks were established across the Longitudinal Valley at Chihshang, Yuli and Juisui (Fig. 13a). The total distances covered by each of these networks fall in the range 5–15 km, while the measured distances vary between 1 and 12 km. The results obtained through repeated geodetic measurements during a period of five years (1983–1988) were presented in detail by Yu and Liu (1989), who also discussed the technical aspects and the uncertainties. As pointed out by Yu et al. (1990), the determinations are reliable because uncertainties are small relative to measured displacements. Accordingly, the data published by Yu and Liu (1989) not only provide estimates of deformation between 1983 and 1988, but also indicate that the fault movements occurred in a rather regular way during this period. Considering these geodetic data, deformation tensors were computed within the networks (Yu and Liu, 1989; Lee and Angelier, 1993). The axis of maxi-

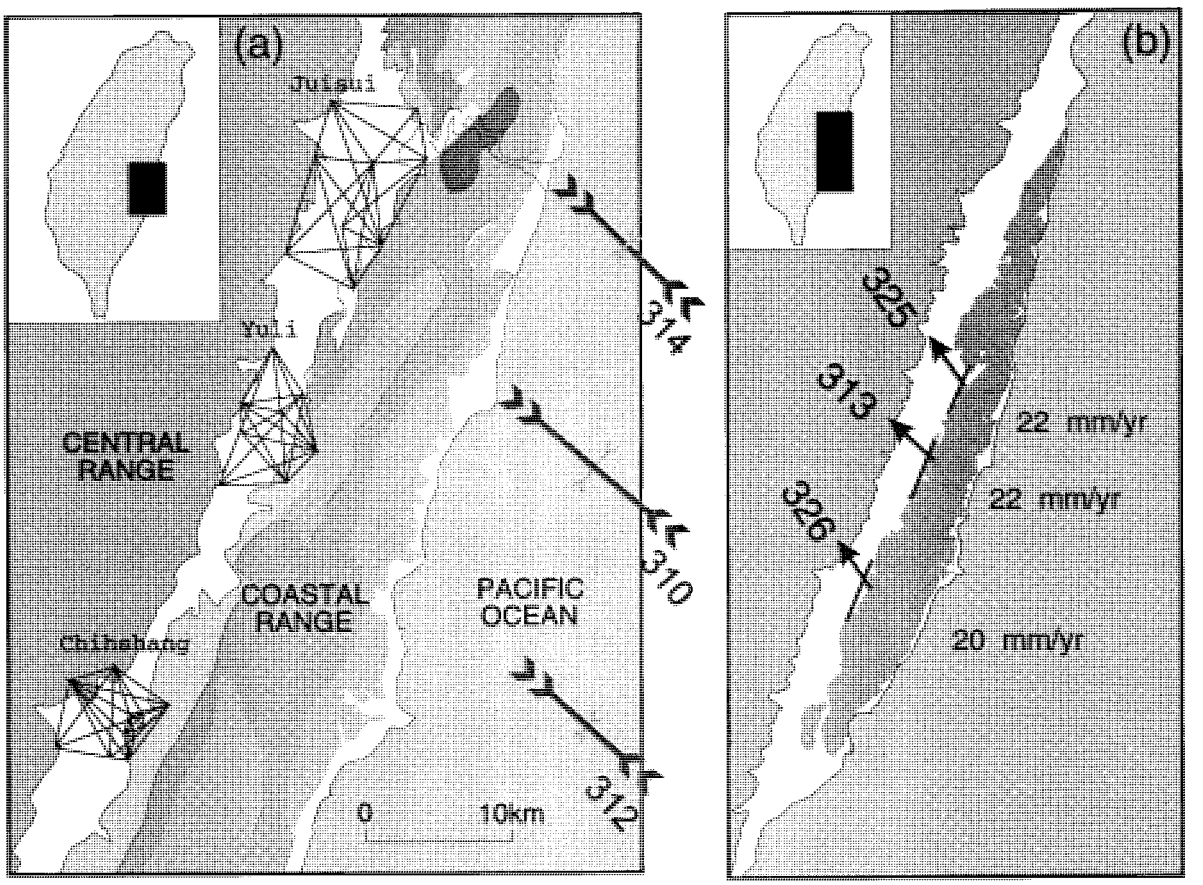

Fig. 13. Deformation and displacement across the Longitudinal Valley active fault zone from Chihshang to Juisui, as reconstructed using the geodetic data from the trilateration networks of Yu and Liu (1989). For location, see Fig. 2. (a) Maps of Chihshang, Yuli and Juisui networks, and axes of maximum and minimum shortening (couples of convergent arrows with double and simple arrowheads, respectively). Computation of 2-D strain tensors by Lee and Angelier (1993). Azimuths of maximum shortening in degrees. (b) Application of models of 'discontinuous deformation' (Lee and Angelier, 1993) to the same geodetic data. Arrows indicate displacement of the upthrust, eastern block of the Longitudinal Valley Fault relative to the Central Range. Computed azimuths of displacement in degrees, computed velocities in mm/yr.

mum shortening trends N132ºE on average for the Chihshang network (Fig. 13a). Very similar values were obtained within the Yuli and Juisui networks, respectively located 23 and 40 km north-northeast of Chihshang, showing that the N132ºE (N48ºW) trend of shortening obtained at Chihshang reflects the tectonic behaviour of the whole Yuli active fault segment (Fig. 13a).

Because the distribution of the displacements within the geodetic networks shows that the deformation is inhomogeneous and occurs along a single major discontinuity considered at a plurikilometric scale, Lee and Angelier (1993) described and used a 'discontinuous model' for analysing geodetic data. In this model, the location, orientation and amplitude of fault slip are the unknowns and they are constrained by the distribution of all distance changes within the geodetic network. Such an analysis, assuming that deformation concentrates on a major fault zone, better accounted for the displacements observed within the networks. The discontinuous model analysis indicated that the average trend of relative displacement is N146ºE (N34ºW) for the Chihshang network, and N141ºE (N39ºW) for the three networks (Fig. 13b). The amounts of displacement thus determined within the three networks for the period 1983–1988 were

found identical within the range of uncertainties (2.1 cm/yr).

These analyses of the 1983–1989 geodetic surveys at Chihshang, Yuli and Juisui thus consistently indicated that across the Longitudinal Valley the eastern block (the Coastal Range) moved with a rather constant velocity of 2.1 cm/yr in the N39ºW direction, relative to the Central Range of Taiwan (Fig. 13b).

4.3. Comparisons with the results of the Global Positioning System survey of Taiwan

The 'Taiwan GPS network' established in 1989 by the Institute of Earth Sciences (Academia Sinica) is composed of 131 annually surveyed stations and 9 continuous monitoring stations. This network provides complete estimates of displacements between the northern tip of the Luzon Arc and the Chinese shelf. The mobile stations were surveyed 3–5 times from 1990 to 1994. The results of these GPS surveys were presented by Yu and Chen (1994) and S.-B. Yu et al. (1995); see also Yu et al., 1997.

At the scale of the Yuli segment of the Longitudinal Valley, we consider the displacement of five stations located on the eastern side (that is, the western flank of the Coastal Range) relative to five stations located on the western side (that is, the eastern flank of the Central Range). We use the data published by Yu and Chen (1994) and S.-B. Yu et al. (1995). For the 1990–1994 period, the average motion vectors of these stations (within a reference frame attached to the Paisha island station of the Chinese shelf and characterized by a constant Paisha–Taipei direction) trend N46ºW and N59ºW for the eastern and western sides of the Longitudinal Valley, respectively. The corresponding velocities are 6.8 cm/yr and 4.3 cm/yr. The consistency is good for each subset. One thus easily calculates within a velocity triangle the movement of the western Coastal Range relative to the eastern Central Range, resulting in a motion vector oriented N25ºW and a velocity of 2.8 cm/yr.

According to the 1990–1994 GPS velocity field obtained by Yu and Chen (1994) and S.-B. Yu et al. (1995), and considering the same reference frame as before, the displacement of the Philippine Sea Plate relative to South China occurs in the N54ºW direction, with a velocity of 8.2 cm/yr (larger than earlier estimates of Philippine Sea–Eurasia convergence, suggesting that South China is not fixed to Eurasia). Comparing the trends of motion vectors on both sides of the Longitudinal Valley with the direction of plate convergence, the movement of the eastern block (the edge of the Coastal Range) deviates 8 degrees clockwise, whereas that of the western block (the edge of the Central Range) deviates 5 degrees counter-clockwise. The sinistral component of motion along the Longitudinal Valley results in partitioning of displacement within the general frame of the N54ºW convergence. This result highlights the role of the Longitudinal Valley Fault zone as a major discontinuity in the deformation field of the collision belt of Taiwan (Hu et al., 1995).

4.4. Comparisons with the results of neotectonic studies in Taiwan

The results obtained at a time scale of about ten years along the active Chihshang Fault deserve comparison with those obtained for the recent Quaternary (Late Pleistocene and Holocene) in the Longitudinal Valley Fault zone and the entire orogen as well (Fig. 1).

First, the deformation of the Quaternary Pinanshan conglomerates (north of Taitung in the Longitudinal Valley) was analysed based on systematic inversion of fault slip data sets (Barrier et al., 1982). This analysis revealed compression trending N100ºE (within the folded conglomerates) and N140ºE (on the eastern side of the Longitudinal Valley).

A regional study of Quaternary compressional deformation was later carried out by similar means, at the scale of the whole Coastal Range of eastern Taiwan (Barrier and Angelier, 1986). The analysis of about 4000 fault measurements collected in more than 60 sites showed that for about 90% of compressional axes the trends range between N90ºE and N140ºE, while for about 25% it is approximately N120ºE.

Summarizing, the Quaternary direction of compression reconstructed within the Longitudinal Valley fault zone and the adjacent Coastal Range is in general agreement with the N132ºE direction of shortening for the present-day activity revealed by geodetic analyses in the Longitudinal Valley. Local deviations occur clockwise and counter-clockwise relative to the N120–132ºE (N48–60ºW) average

trend of compression, because of regional dispersion, inhomogeneity in geological structure, stress-strain partitioning and block rotation.

At the scale of the Taiwan orogen, the directions of compression related to Quaternary shortening and the general direction of the plate convergence are similar. However, significant deviations occur and trajectories are fan-shaped in the fold-and-thrust belt as revealed by reconstructions of the Quaternary stress field (Angelier et al., 1986). The dominating trend of Quaternary compression, N122ºE (N58ºW) in central Taiwan, undergoes deviations as large as 40º clockwise (to the north) and 20º counter-clockwise (to the south).

In order to check in a mechanically consistent way the overall relationship between the orientation of plate convergence and the distribution of compressional trajectories throughout the belt, finite-element numerical modelling was used (Hu et al., 1996). In contrast, the distinct-element modelling (Hu et al., 1995) principally aimed at evaluating the role of the major discontinuities such as for the Longitudinal Valley Fault and the front thrusts. It is certainly significant that the dominating trend of Quaternary compression in the Foothills of central Taiwan is nearly parallel to the present-day direction of shortening reconstructed 100 km to the southeast based on the geodetic analyses in the Longitudinal Valley.

5. Discussion and conclusion

From the methodological point of view, our study demonstrates that it is possible to obtain reliable annual records of displacement based on detailed surveys of partly buried, massive concrete structures. Among the limitations, we especially mention the indispensable severe selection of sites, based on the geometrical requirements discussed earlier in this paper. As a result, only three sites were extensively and repeatedly analysed, although evidences of active faulting are numerous along the Chihshang Fault. Another limitation, illustrated by differences in orientation of fault slip along the Chihshang Fault, is the necessity to study several sites because the fault behaviour may vary along strike.

On the contrary, these analyses provide an accurate record of the local fault kinematics and the variations can be analysed during periods of several years. Of particular interest, in this respect, are the variations of local displacement with time, indicating that the shortening velocity across the Chihshang Fault decreased in 1993 (Figs. 6, 9 and 12). Thus, local quantitative studies carried out along active faults have the potential to allow detection of a decrease in aseismic slip velocity for a given fault, a warning which may suggest accumulation of compressional strain across a nearby zone, and consequently an increasing earthquake hazard within an area where overall deformation is continuing. Studies at wider scales do not have this potential as far as successive faults develop in a relatively narrow zone. The possible situation of accumulating stress should be considered in the near future for the Chihshang Fault if the forthcoming analyses reveal that the decrease in velocity noticed in 1993–1994 is continuing. However, the destruction, in 1994, of the concrete structures used as bench-marks in the northern two sites makes further surveying more difficult.

From the tectonic point of view, our local results constrain the behaviour of the active Chihshang Fault. In terms of horizontal components of deformation, the fault generally strikes N18ºE whereas the average motion vectors that we determined trend N37ºW. Because we determined an average shortening of 2.2 cm/yr, this angle of 55º between the fault strike and the trend of relative displacement indicates that the transverse component of motion (related to westward thrusting) is 1.8 cm/yr, whereas the strike-slip component of motion is 1.3 cm/yr. These values are in agreement with those determined by Lee and Angelier (1993) using the geodetic data of Yu and Liu (1989), that is 1.8 cm/yr and 1.1 cm/yr, respectively.

In terms of vertical components of motion, the dip of the fault should be determined first. Considering the average plunge, δ, of all motion vectors at the Tapo and Chinyuan sites, and taking into account the obliquity of their trends relative to fault strikes (55º), one determines the dip θ of the fault, given by $\tan(\theta) = \tan(\delta)/\sin 55^\circ$. With $\delta = 34^\circ$, one obtains $\theta = 39^\circ$. This local determination, based on our orientation measurements, is supported by the seismic data which suggest an average value of 45º eastward for the dip of the Longitudinal Valley fault zone (Tsai, 1986). It is likely that the Chihshang Fault dips about 40º eastward.

With the value of 1.8 cm/yr determined above for the transverse component of horizontal shortening, this estimation of fault dip implies that the vertical displacement velocity averages 1.5 cm/yr. This value is about one half of that indicated by the levelling studies carried out in 1986–1988 across the Chihshang Fault (Yu and Liu, 1989). We suspect that the latter value denotes an abnormally fast rate related to a period of downwarping in the downthrown side of the fault, as suggested by the later contrasting evolution at the site between Tapo and Chinyuan. Considering the uncertainties, we conclude that these rates of vertical displacement, 1.5 and 3 cm/yr, are compatible in a first approximation.

These determinations of components of relative displacement of the Chihshang Fault (1.8 cm/yr for transverse shortening, 1.3 cm/yr for sinistral slip and 1.5 cm/yr for vertical motion) imply that the actual offset of the fault (counted along the motion vector) increases at a rate of 2.7 cm/yr on average (with 3 cm/yr for vertical motion, one would obtain 3.7 cm/yr).

The local trend of relative displacement across the Chihshang Fault, N37ºW on average, is in agreement with those reconstituted within the 6-km-wide Chihshang geodetic network across the Valley (N34ºW) or the three networks shown in Fig. 13 (N39ºW). In terms of shortening velocities, the values are identical (2.1–2.2 cm/yr). These comparisons show that the shortening across the Longitudinal Valley is concentrated on the single Chihshang Fault. Analyses of data obtained in 10 GPS stations on both sides of the valley indicate a higher relative velocity, 2.8 cm/yr, in the N25ºW direction. This result is still consistent, because such estimates deal with a larger zone and include additional shortening on valley sides.

The Longitudinal Valley Fault is not a fixed boundary. Far to the north, the active fault does not follow the geological fault zone separating the Coastal Range and the Central Range of Taiwan, but crosses obliquely the Coastal Range and merges into the offshore active tectonic zone that separates the Taiwan collision belt and the westernmost portion of the Ryukyu subduction zone (Angelier et al., 1995a,b). Thus, during the late Quaternary the northernmost portion of the Longitudinal Valley Fault was abandoned as a site of reverse-sinistral shear concentration, whereas to the south it remained the major active plate boundary.

An other important aspect of deformation distribution deals with the tectonic behaviour of the Chihshang Fault (as part of the Yuli segment of the Longitudinal Valley Fault), as an oblique front thrust of one of the units of the Coastal Range. These units rotated clockwise of about 20–30º during the collision of the Luzon Arc (trending N10ºW) with the Central Range, as revealed by palaeomagnetic studies (Lee, 1989). This phenomenon resulted from the adaptation of the Luzon Arc thrust units to the orientation of the Central Range, and resulted in segmentation of the Coastal Range and Longitudinal Valley Fault. Right-lateral transcurrent faults developed between these segments in order to accommodate the general left-lateral movement related to oblique thrusting (Fuh et al., 1994). The particular behaviour of the active Chihshang Fault as a thrust with increasing left-lateral component near fault tips is probably influenced by this segmentation: the active Chihshang Fault might be a sigmoidal fault segment bounded by a transcurrent fault near its end, which would explain the significant difference between motion vector trends at the tips and in the intermediate site.

In terms of tectonic strain and stress, there is an excellent fit between the trends of the maximum compression calculated within the geodetic networks (Fig. 13a), from the fault slip data analyses carried out throughout the Longitudinal Valley–Coastal Range, and even in the Central Foothills of Taiwan (100 km to the northwest, on the opposite side of the collision belt). These trends are N48ºW, N60ºW and N58ºW, respectively.

This homogeneous orientation of compression along a NW–SE axis across the central collision zone (Fig. 1) is remarkably consistent with the N54ºW trend of convergence between the northernmost Luzon Arc and South China revealed by GPS studies (S.-B. Yu et al., 1995). It is also consistent with the average compressional trends indicated by earthquake focal mechanism analyses in the Taiwan region (Yeh et al., 1991).

Our study provides an example of extreme shear concentration in an oblique collision zone. The small-scale observations and measurements presented in this paper yielded the single possible

evidence that large fault motion concentrates in a narrow zone (less than 1% of the total fault zone width). The horizontal shortening of the Longitudinal Valley Fault at Chihshang, 2.2 cm/yr on average, occurs across a single fault zone, which consists of a unique fault or narrowly spaced branches. The whole reverse slip (about 2.7–3.7 cm/yr depending on fault dip) was entirely recorded by walls 20–200 m long, where faults are tightly localized. This active fault accounts for more than one fourth (27%) of the total shortening between the Luzon Arc and South China recorded through GPS analyses (S.-B. Yu et al., 1995).

Motion on the Chihshang fault occurs principally through creeping and no large earthquake occurred recently. The 1951 earthquakes probably played a large role and initiated the subsequent period of creeping with large strain rates (generally larger than $1 \cdot 10^{-3}$/yr considering the width of the fault zone). The decreasing motion velocity illustrated in Figs. 6, 9 and 12, if significant, may announce a new stage of fault locking and increasing compressional stress, 45–50 years later: a situation which would reveal increasing earthquake risk and deserves attention. Despite practical difficulties related to wall reconstructions, our forthcoming surveys are important in this respect, because of their potential to reveal whether fault locking is really increasing, or creeping and 'weak' fault behaviour continuing.

Acknowledgements

This work was carried out within the frame of the Sino–French cooperation program in Earth Sciences. The help of the Institut Français à Taipei (I.F.T.), the National Science Council of Taiwan (N.S.C.), the French program 'P.N.T.S.', the Central Geological Survey of Taiwan (C.G.S.), and the Institut Français du Pétrole (I.F.P.) is gratefully acknowledged.

References

Angelier, J., 1986. Geodynamics of the Eurasia–Philippine Sea Plate boundary: preface. Tectonophysics, 125(1–3): IX–X.

Angelier, J., Barrier, E. and Chu, H.-T., 1986. Plate collision and paleostress trajectories in a fold-thrust belt: the Foothills of Taiwan. Tectonophysics, 125: 161–178.

Angelier, J., Chu, H.-T. and Lee, J.-C., 1995a. Shear concentration in a collision zone: kinematics of the active Chihshang Fault, Longitudinal Valley, eastern Taiwan. In: H.-H. Tsien (Editor), ACT Int. Conf., Ext. Abstr. Geol. Soc. China Spec. Publ., Taipei, pp. 17–24.

Angelier, J., Lee, J.-C., Chu, H.-T., Lu, C.-Y., Fournier, M., Hu, J.-C., Lin, N.-T., Deffontaines, B., Delcaillau, B., Lacombe, O. and Lee, T.-Q., 1995b. Crustal extension in an active orogen: Taiwan. In: H.-H. Tsien (Editor), ACT Int. Conf., Ext. Abstr. Geol. Soc. China Spec. Publ., Taipei, pp. 25–32.

Barrier, E. and Angelier, J., 1986. Active collision in eastern Taiwan: the Coastal Range. Tectonophysics, 125: 39–72.

Barrier, E. and Chu, H.-T., 1984. Field trip guide to the Longitudinal Valley and the Coastal Range in eastern Taiwan. In: Field Guidebook for the Sino–French Colloquium on Geodynamics of Eurasia–Philippine Sea Plate Boundary, Taipei, pp. 27–49.

Barrier, E., Angelier, J., Chu, H.-T. and Teng, L.-S. 1982. Tectonic analysis of compressional structure in an active collision zone: the deformation of the Pinanshan Conglomerates, eastern Taiwan. Proc. Geol. Soc. China, 25: 123–138.

Bonilla, M.G., 1977. Summary of Quaternary faulting and elevation changes in Taiwan. Mem. Soc. Geol. China, 2: 43–56.

Chu, H.-T., Lee, J.-C. and Angelier, J., 1994. Non-seismic rupture of the Tapo and the Chinyuan area on the southern segment of the Huatung Longitudinal valley fault, Eastern Taiwan. Soc. Geol. China, Annual Meeting, Taipei, 25–26 March 1994. Coll. Abstracts, pp. 1–5.

Fuh, S.-C., Liu, C.-S. and Song, J.-S., 1994. Decoupled transcurrent faults in the offshore area south of Taiwan. Pet. Geol. Taiwan, 29: 27–46.

Ho, C.-S., 1986. A synthesis of the geologic evolution of Taiwan. Tectonophysics, 125: 1–16.

Hsu, T.-L., 1962. Recent faulting in the Longitudinal Valley of eastern Taiwan. Mem. Geol. Soc. China, 1: 95–102.

Hu, J.-C., Angelier, J., Yu, S.-B. and Lu, C.-Y., 1995. An interpretation of the GPS Velocity field of southern Taiwan based on numerical modelling. In: H.-H. Tsien (Editor), ACT Int. Conf., Ext. Abstr. Geol. Soc. China Spec. Publ., Taipei, pp. 141–149.

Hu, J.-C., Angelier, J., Lee, J.-C., Chu, H.-T. and Byrne, D., 1996. Kinematics of convergence, deformation and stress distribution in the Taiwan collision area: 2-D finite-element modelling. Tectonophysics, in press.

Lee, J.-C., 1994. Structure et déformation active d'un orogène: Taiwan. Mém. Sci. Terre Univ. P. et M. Curie, Paris, 94-17, 281 pp.

Lee, J.-C. and Angelier, J., 1993. Localisation des déformations actives et traitement des données géodésiques: l'exemple de la faille de la Vallée Longitudinale, Taiwan. Bull. Soc. Géol. Fr., 164(4): 533–570.

Lee, T.-Q., 1989. Evolution tectonique et géodynamique néogène et quaternaire de la chaîne côtière de Taiwan: apport du paléomagnétisme. Mém. Sci. Terre Univ. P. et M. Curie, Paris, 89-X, 328 pp.

Tsai, Y.-B., 1986. Seismotectonics of Taiwan. Tectonophysics, 125: 17–37.

Yeh, Y.-H., Barrier, E., Lin, C.-H. and Angelier, J., 1991. Stress tensor analysis in the Taiwan area from focal mechanisms of earthquakes. Tectonophysics, 200: 267–280.

York, J.-E., 1976. Quaternary faulting in eastern Taiwan. Bull. Geol. Surv. Taiwan, 25: 63–72.

Yu, M.-S., Cheng, S.-N. and Liew, P.-M., 1995. The seismotectonic activity of the Yuli segment, Taitung Longitudinal Valley. In: H.-H. Tsien (Editor), ACT Int. Conf., Ext. Abstr. Geol. Soc. China Spec. Publ., Taipei, pp. 309–315.

Yu, S.-B. and Chen, H.-Y., 1994. Global Positioning System measurements of crustal deformation in the Taiwan arc–continent collision zone. Terrestrial, Atmospheric and Oceanic Sci., 5: 477–498.

Yu, S.-B. and Liu, C.-C., 1989. Fault creep on the central segment of the Longitudinal Valley Fault, Eastern Taiwan. Proc. Geol. Soc. China, 32(3): 209–231.

Yu, S.-B. and Tsai, Y.-B., 1982. A study of microseismicity and crustal deformation of the Kuangfu–Fuli area in eastern Taiwan. Bull. Inst. Earth Sci. Acad. Sin., 2: 1–18.

Yu, S.-B., Jackson, D.-D., Yu, G.-K. and Liu, C.-C., 1990. Dislocation model for crustal deformation in the Longitudinal Valley area, Eastern Taiwan. Tectonophysics, 183: 97–109.

Yu, S.-B., Chen, H.-Y. and Kuo, L.-C., 1995. Velocity field of GPS Stations in the Taiwan area. In: H.-H. Tsien (Editor), ACT Int. Conf., Ext. Abstr. Geol. Soc. China Spec. Publ., Taipei, pp. 317–327.

Yu, S.-B., Chen, H.-Y. and Kuo, L.-C., 1997. Velocity field of GPS stations in the Taiwan area. In: S.E. Lallemand and H.-H. Tsien (Editors), Active Collision in Taiwan. Tectonophysics, 274: 41–59 (this issue).